Deep Adsorption Desulfurization of Fluid Catalytic Cracking Light Gasoline on NiO/ZnO-TiO$_2$ Adsorbents with a High Breakthrough Sulfur Capacity

Guanglin Zhou, Sheng Chen, Weili Jiang,* Qin Li, Hongjun Zhou, Xuecheng Gong, and Xiance Zhang

Read Online

ACCESS | Metrics & More | Article Recommendations
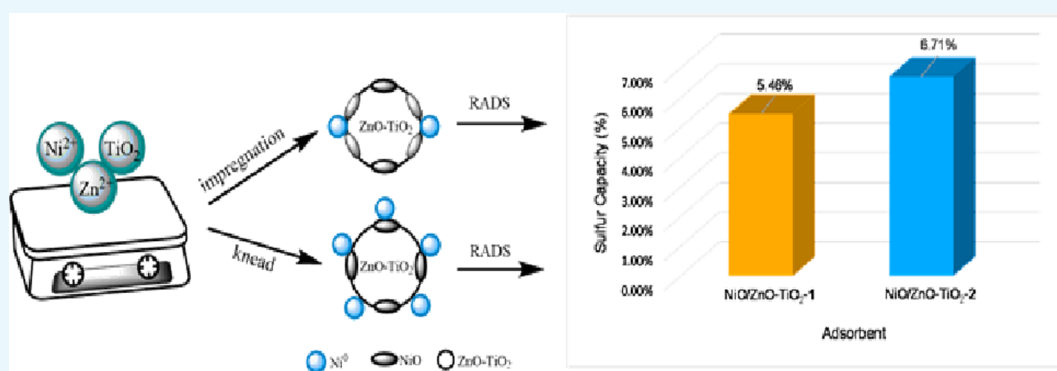
ABSTRACT: Two kinds of NiO/ZnO-TiO$_2$ adsorbents were prepared by equal volume impregnation (NiO/ZnO-TiO$_2$-**1**) and kneading (NiO/ZnO-TiO$_2$-**2**) methods. The adsorbents were characterized by X-ray diffraction, mercury intrusion porosimetry, scanning electron microscopy, energy dispersive X-ray spectroscopy, H$_2$ temperature-programmed reduction, and H$_2$ temperature-programmed desorption. It was found that NiO/ZnO-TiO$_2$-**2** had a smaller average pore diameter and a larger specific surface area as well as a more uniform distribution of the nickel element. Additionally, more Ni^0 active sites together with a stronger interaction between the active component and the support were detected on the surface of NiO/ZnO-TiO$_2$-**2**, which was beneficial to the inhibition of olefin saturation during desulfurization. The desulfurization performance of the adsorbents was investigated in a fixed bed reactor with fluid catalytic cracking light gasoline as a feed oil. The evaluation results confirmed NiO/ZnO-TiO$_2$-**2** with a better desulfurization performance with less olefin saturation. It could reduce the total sulfur content from 300 ppmw to less than 5 ppmw, and the breakthrough time and breakthrough sulfur capacity were 91 h and 6.71% (67.1 mg S/g adsorbent), respectively.

1. INTRODUCTION

As the demand for transportation fuel has been increasing in most countries in the past few decades, automobile emissions have become a significant source of air pollution,[1−3] and thus more stringent gasoline standards have been put forward around the world.[4,5] For example, in China, the United States, and Europe, the sulfur content in gasoline is required to be lower than 10 mg/kg.

The sulfides in gasoline usually include mercaptan, thioether, thiophene, and their derivatives.[6−8] Mercaptans and thioethers can be removed through traditional desulfurization technologies such as hydrodesulfurization (HDS)[9−11] and non-hydrodesulfurization.[12,13] Thiophene, however, is difficult to remove through traditional hydrodesulfurization because the conjugate structure formed by coplanar carbon and sulfur atoms makes the C−S bond difficult to break.[1,14,15] Additionally, the traditional desulfurization process is usually accompanied by olefin hydrogenation, which will lead to a reduction

in gasoline octane number.[16−18] Thus, new ultradeep desulfurization technologies are needed to produce clean gasoline.[19,20] An S-Zorb process developed by Conoco Phillips Co. is a widely used technology for producing ultralow-sulfur full-range gasoline.[21] This process combines the advantages of HDS and adsorption desulfurization, which can effectively remove sulfur compounds through reactive adsorption desulfurization (RADS) using Ni/ZnO-based adsorbents while maintaining the octane number.[22−25]

Babich and Moulijn investigated the removal mechanism of thiophene on NiO/ZnO.[26] Ullah et al.[27] studied the possible

Table 1. Properties of Lanzhou Petrochemical Catalytic Cracking Light Gasoline

sulfur content (ppmw)	octane number (RON)	hydrogen sulfide (mg/L)	thiosulfide (mg/L)	mercaptan sulfur (mg/L)	thiophene (mg/L)	total sulfur content (mg/L)
20	94.9	0.08	1.32	0.54	17.68	19.62
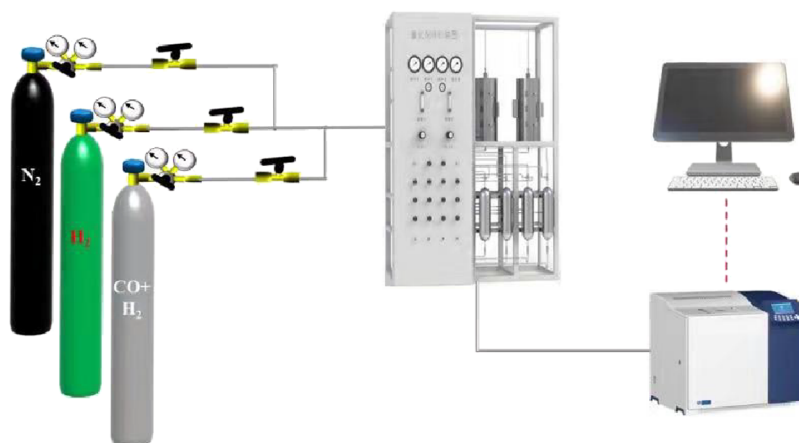
Figure 1. Schematic diagram of the fixed bed reactor.

RADS mechanism proposing that the key to prepare high-performance adsorbents lied in adsorbents with a high dispersion of metal components and a highly porous structure. Meng et al.[28] compared the adsorption desulfurization performance of Ni/ZnO-based adsorbents supported on different supports, finding that the high dispersion of the active components and weak interactions between the active components and the support were beneficial for a better RADS performance. Huang et al.[29] prepared Ni/ZnO adsorbents with various Ni/Zn molar ratios and found that the Ni content played a vital role in determining the RADS activity of Ni/ZnO.

It is known that more than three-quarters of commercial gasoline for automobiles in China is FCC (fluid catalytic cracking) light gasoline, where the olefin content is usually over 40%.[30] The S-Zorb process is not suitable for FCC light gasoline desulfurization because the olefins are easily hydrogenated to saturate, reducing the octane number of gasolines. So far as we know, little work has been reported on the deep desulfurization of FCC light gasoline, without losing its octane number. Zhou et al.[31] discovered that a suitable amount of TiO$_2$ could promote the sulfidation of Ni species, which would further facilitate the formation of NiMoS active phases, making NiMo/MA-Ti a superior catalyst. In our previous study, it was proven that doping of Ti could improve the dispersion of the active component Ni in the Ni/ZnO adsorbent, increase the number of Ni active sites, and thus enhance the desulfurization performance.[32]

At present, the penetrating sulfur capacity of most adsorbents is about 40 mgS/g. Herein, two kinds of Ni/ZnO-TiO$_2$ adsorbents were prepared by a kneading method and an impregnation method for FCC light gasoline reactive adsorption desulfurization. The adsorbents were characterized by XRD, H$_2$-TPR, H$_2$-TPD, and mercury intrusion. Their effects on desulfurization performances were studied, where it showed that the one prepared by a kneading method had a larger breakthrough sulfur capacity.

2. EXPERIMENTAL SECTION

2.1. Materials. The FCC light gasoline was obtained from Lanzhou Petrochemical Company. The composition and the basic properties of the gasoline are listed in Table 1. In order to shorten the experimental period, thiophene was added to the feed oil to increase the sulfur content, and the total sulfur content of the feed oil was set to 300 ppmw.

Zinc oxide (industrial grade), a pore-forming agent (carboxymethylcellulose, industrial grade), and titanium dioxide (industrial grade) were purchased from Shandong Zibo Hengyi Chemical Technology Co., Ltd. Nickel nitrate (chemical pure grade) was purchased from Hubei Xinrunde Chemical Co., Ltd., and citric acid (analytical reagent grade) was purchased from Shanghai Dingxu Chemical Co., Ltd. Nitric acid (analytical reagent grade, 65.0−68.0%) was purchased from Sinopharm Chemical Reagent Co., Ltd.

2.2. Preparation of Adsorbents. *2.2.1. Equal Volume Impregnation Method.* Zinc oxide (95.00 g) was mixed with titanium dioxide (5.00 g) and the pore-forming agent (2.00 g). Dilute nitric acid solution (1.8 wt %, 40.00 g) was then added to the mixed powder and stirred. After kneading in a squeezer for 90 min, the template was extruded and dried at room temperature for 12 h. After being dried at 120 °C for 3 h, it was calcined in the air at 500 °C for 3 h to give the ZnO-TiO$_2$ support. Next, a solution was prepared by dissolving 14.68 g of nickel nitrate and 4.60 g of citric acid in deionized water. The ZnO-TiO$_2$ support was impregnated with the above solution through an equal volume impregnation method. After being dried at 120 °C for 3 h, the solid was calcined at 500 °C for 3 h to obtain the Ni/ZnO-TiO$_2$-**1** adsorbent with a Ni loading of 4.45 wt %.

2.2.2. Kneading Method. Zinc oxide powder (95.00 g) was mixed with nickel nitrate (14.68 g), citric acid (4.60 g), the pore-forming agent (2.00 g), and titanium dioxide (5.00 g). Dilute nitric acid solution (1.8 wt %, 40.00 g) was then added to the above mixture and mixed well. After kneading in a squeezer for 90 min, the template was extruded and the solid was dried at room temperature for 12 h. The sample was then dried at 120 °C for 3 h before being calcined in the air at 500
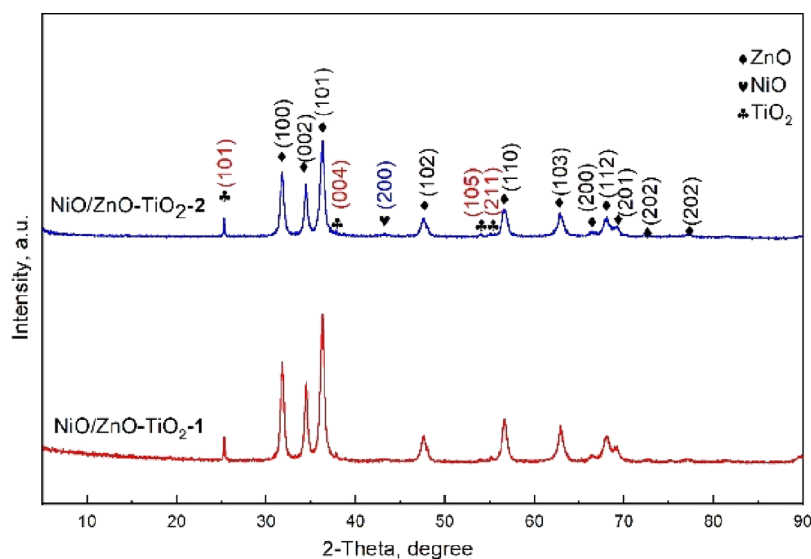
Figure 2. XRD spectra of the two $NiO/ZnO-TiO_2$ adsorbents.

Table 2. Surface and Pore Properties of the Two $NiO/ZnO-TiO_2$ Adsorbents

adsorbents	S_{BET} $(m^2 \cdot g^{-1})$	pore volume $(mL \cdot g^{-1})$	average aperture (nm)	bulk density $(g \cdot cm^{-3})$	particle strength (N/cm)
$NiO/ZnO-TiO_2$-**1**	30.34	0.24	32.70	1.3	78.4
$NiO/ZnO-TiO_2$-**2**	31.02	0.23	29.60	1.3	65.7

°C for 3 h to form the $Ni/ZnO-TiO_2$-**2** adsorbent with a Ni loading of 4.45 wt %.

2.3. Characterization of Adsorbents. XRD patterns were obtained on a D8 Advance type X-ray diffractometer (Cu Kα, λ = 1.54051 Å) in a scanning range of 2θ = 5 to 90°. A mercury intrusion test was carried out on an Autopore IV 9510 automatic mercury injector with a mercury intrusion pressure range of 0.1 to 60000.0 psia. H_2-TPR spectra were measured using an AutoChem II 2920 automatic analyzer. The samples were placed in the air at 500 °C for 2 h and cooled in an Ar atmosphere. Then, temperature-programmed reduction was carried out in a mixed gas stream of Ar/H_2 (90/10 mol/mol, 50 mL/min) at a heating rate of 10 °C/min to 700 °C. The samples were reduced in a hydrogen atmosphere for 2 h. After cooling to 50 °C, hydrogen was adsorbed for 1 h and purged with Ar for 1 h. The temperature-programmed desorption was carried out at a heating rate of 10 °C/min to 550 °C.

2.4. Desulfurization Experiments. The FCC light gasoline desulfurization reaction was carried out in a 15 mL fixed bed reactor loaded with 15 mL of adsorbent (Figure 1). The experiment was performed at 340 °C under a pressure of 0.6 MPa. Prior to the reaction, the adsorbent was reduced by hydrogen at 350 °C and 0.5 MPa for 2 h. Then, the gasoline was introduced into the reactor at a weight hourly space velocity (WHSV) of 5 h^{-1} with a H_2/oil volume ratio of 25. The outlet product was collected for analysis every 2 h. The sulfur content in the gasoline was detected on an RPP-2000S ultraviolet fluorescence sulfur analyzer. When the sulfur content of the product exceeded 5 ppmw, the adsorbent was considered to be broken through and the reaction would be stopped. The breakthrough sulfur capacity (S_C, the amount of sulfur that can be absorbed by a unit volume desulfurizer) was determined as follows:

$$S_C = \frac{Q \times \rho \times (C_{in} - C_{out}) \times t \times 10^{-6}}{m} \times 100\%$$

In the formula, Q is the gasoline flow rate (mL/h), ρ is the gasoline density (g/mL), t is the breakthrough time (h), m is the mass of the adsorbent (g), and C_{in} and C_{out} are the sulfur contents (ppmw) in the inlet and outlet gasoline.

3. RESULTS AND DISCUSSION

3.1. XRD Analysis. The XRD spectra of the two $Ni/ZnO-TiO_2$ adsorbents are shown in Figure 2. It can be seen that the XRD patterns of the two adsorbents were similar, indicating that they had the same compositions, which were NiO, TiO_2, and ZnO. The peaks at 31.77, 34.42, 36.26, 47.54, 56.60, 62.85, 67.95, 69.09, and 72.57° were classified as ZnO (ICDD-PDF No. 65-3411). The diffraction peaks of rutile TiO_2 (ICDD-PDF No. 21-1272) were found at 25.28, 37.77, 53.88, and 55.01°. The weak diffraction peak that appeared at 43.1° was attributed to the crystalline NiO,[33] which was generated from the decomposition of the $Ni(NO_3)_2$ precursor. The diffraction peaks attributed to NiO of the two absorbents were extremely weak, suggesting that NiO was highly dispersed on the supports.

3.2. Physical Properties of Adsorbents. The surface and pore properties of the two $NiO/ZnO-TiO_2$ adsorbents are shown in Table 2 and Figure 3. It can be seen from Table 2 that the internal pores of the adsorbents were mainly distributed at 10−50 nm, which was a typical mesoporous structure. The distribution ratio of pores at 10−25 nm of $NiO/ZnO-TiO_2$-**2** was higher than that of $NiO/ZnO-TiO_2$-**1**, while $NiO/ZnO-TiO_2$-**1** had a higher pore distribution ratio at 25−50 nm. This resulted in the average pore sizes of $NiO/ZnO-TiO_2$-**1** being larger than those of $NiO/ZnO-TiO_2$-**2**, which were 32.70 and 29.60 nm, respectively. At the same time, the specific surface area of $NiO/ZnO-TiO_2$-**2** was slightly larger, which was 31.02 $m^2 \cdot g^{-1}$. The difference in the pore distribution might be explained by the different preparation methods. In the kneading method, the precursor of the active
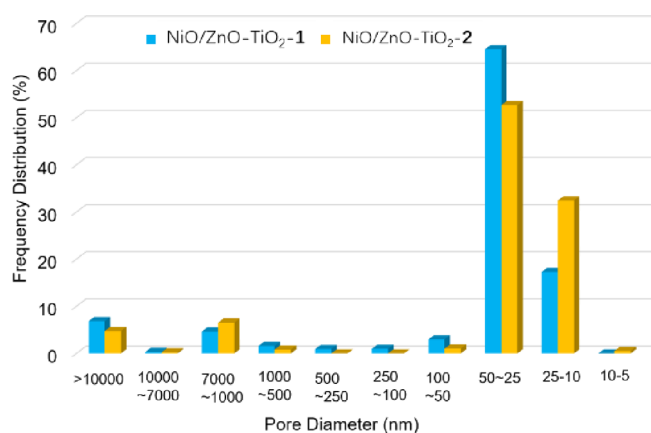
Figure 3. Pore diameter distribution of the two NiO/ZnO-TiO$_2$ adsorbents.

component was uniformly mixed with the powder mixture of the prepared support in the form of a solution. The molding adsorbent was obtained by direct extrusion and calcination. The active species was dispersed more uniformly on the support, and at the same time, it participated in the formation of the support pores. As to the impregnation method, the support had been calcined to form a certain pore structure. When the support was impregnated with the active precursor solution, the active species might accumulate and grew inside the pores. This caused damage or blockage to smaller channels, resulting in increased channels. It can also be seen from Table 3 that the particle strength of NiO/ZnO-TiO$_2$-**2** was relatively low.

Table 3. Breakthrough Sulfur Capacities of the Two Ni/ZnO-TiO$_2$ Adsorbents

sample	sulfur capacity (%)
NiO/ZnO-TiO$_2$-**1**	5.46
NiO/ZnO-TiO$_2$-**2**	6.71

3.3. Morphology and Composition Analysis.

The morphology and composition of the two adsorbents were studied through SEM and EDX characterization, listed in Figure 4. Not so much difference could be observed on their SEM pictures, meaning that the two adsorbents have similar surface topography. The EDX results, however, gave more interesting information. First, the composition of the two adsorbents were nearly the same, i.e., with 13−14% Ti, 11−12% Ni, and 74−75% Zn. Nevertheless, one obvious difference was discovered in the distribution of the Ni element. The nickel element in NiO/ZnO-TiO$_2$-**1** was very concentrated, while that in NiO/ZnO-TiO$_2$-**2** dispersed very well.

3.4. H$_2$-TPR Analysis.

The reduction performances of the adsorbents were investigated through H$_2$-TPR experiments, and the results are demonstrated in Figure 5. It is found that
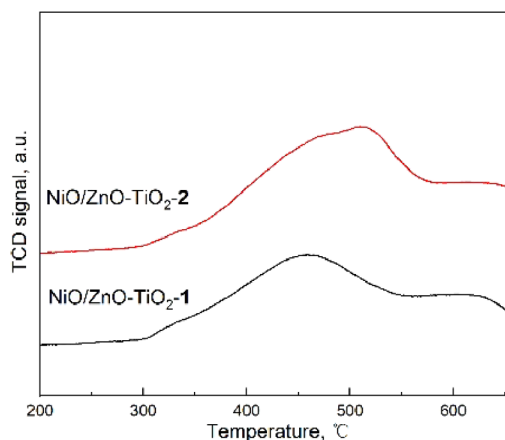
Figure 5. H$_2$-TPR of the two NiO/ZnO-TiO$_2$ adsorbents.

the two H$_2$-TPR curves had a similar tendency, with a broad band at 300−550 °C and a weak shoulder band around 330 °C, which belonged to the reduction of NiO species.[34] The lower temperature bands were attributed to the weak
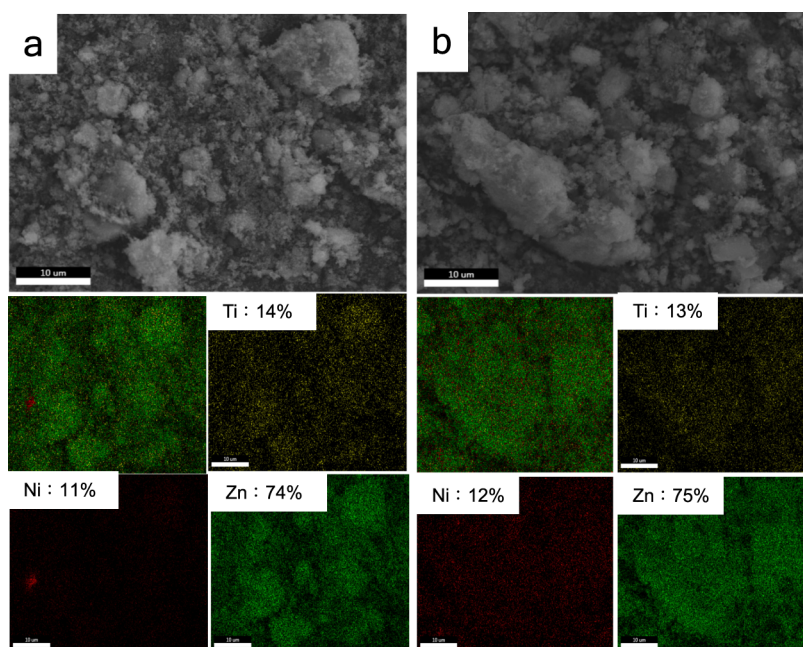
Figure 4. SEM and EDX results of (a) NiO/ZnO-TiO$_2$-**1** and (b) NiO/ZnO-TiO$_2$-**2**.

interaction between Ni^{2+} species and the $ZnO-TiO_2$ support, while the higher temperature signals were attributed to the strong interaction of Ni^{2+} and the support.[35] The reduction band of $NiO/ZnO-TiO_2$-**2** shifted toward the higher temperature, which implied that there is a stronger interaction between the Ni species and this support than $NiO/ZnO-TiO_2$-**1**. That is, the NiO species in $NiO/ZnO-TiO_2$-**2** was more difficult to reduce. At the same time, the enhancement of metal−support interaction also reduced the amount of free NiO, which was beneficial to the inhibition of the olefin saturation reaction in the desulfurization process.[36] In addition, the reduction peak area of $NiO/ZnO-TiO_2$-**2** (19.8) was larger than that of $NiO/ZnO-TiO_2$-**1** (12.4), suggesting that the former contained more NiO component that could be reduced, which might be generated in $NiO/ZnO-TiO_2$-**2** under suitable reduction conditions.

3.5. H_2-TPD Analysis. The adsorbents were further characterized by H_2-TPD (Figure 6) in order to study the
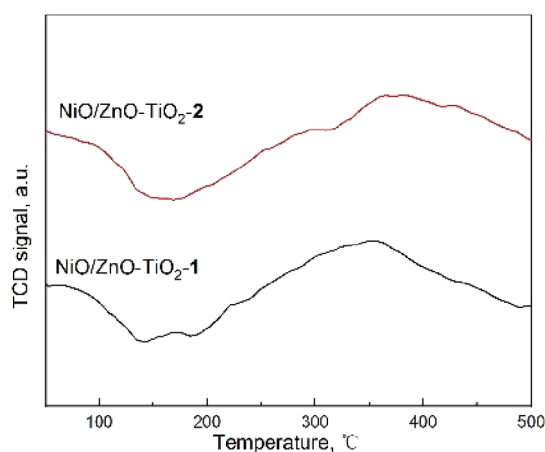
Figure 6. H_2-TPD profiles of the $Ni/ZnO-TiO_2$ adsorbents by different methods.

dispersion state of surface Ni^0 species on the adsorbents after reduction. It can be found that both of the adsorbents showed a low-temperature hydrogen desorption peak at 50−140 °C and a high-temperature peak at a range higher than 200 °C. The lower-temperature peak was generally related to the desorption of hydrogen adsorbed on the surface active species Ni^0 of the adsorbent support,[37,38] and the area of the desorption peak was positively correlated with the amount of surface active species Ni^0. By calculation, the hydrogen desorption peak area of $NiO/ZnO-TiO_2$-**2** (0.142) was larger than that of $NiO/ZnO-TiO_2$-**1** (0.063), indicating that more active Ni^0 sites were generated on the former after reduction. Together with the EDX results in Figure 4, the possible reason was that for $NiO/ZnO-TiO_2$-**1**, the active component impregnation was uneven during the impregnation process, which thus caused a large amount of agglomeration of nickel, resulting in fewer active sites. In addition, according to Table 2, $NiO/ZnO-TiO_2$-**2** had a smaller average pore diameter and a larger specific surface area, which helped to support more active sites of Ni^0.

3.6. Adsorption Desulfurization Performance of the Adsorbents. The adsorption desulfurization performances of the two $Ni/ZnO-TiO_2$ adsorbents were tested with FCC light gasoline, and the results are shown in Figure 7 and Table 3. As revealed, both of the adsorbents had an excellent desulfuriza-
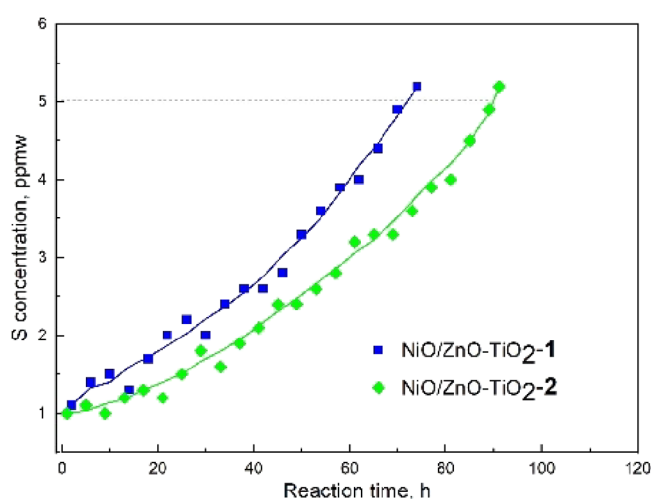
Figure 7. Breakthrough curves for adsorptive desulfurization of FCC gasoline on the two $Ni/ZnO-TiO_2$ adsorbents.

tion performance, and the sulfur content in the FCC light gasoline could be removed to below 5 ppmw for a long time. The desulfurization performance of $NiO/ZnO-TiO_2$-**2** was more superior with a breakthrough time of 91 h and breakthrough sulfur capacity of 6.71% (67.1 mg S/g adsorbent). Compared with 74 h and 5.46% (54.6 mg S/g adsorbent) for $NiO/ZnO-TiO_2$-**1**, the breakthrough sulfur capacity of $NiO/ZnO-TiO_2$-**2** was increased by 23%. Considering the slightly stronger interaction between the support, which would make the NiO species in the adsorbent more difficult to be reduced, together with the more active species Ni^0 for $NiO/ZnO-TiO_2$-**2**, the interaction strength should not have a big impact on the desulfurization performance. The possible reason was that the relatively large specific surface area of $NiO/ZnO-TiO_2$-**2** was beneficial to support more active sites on the surface, which was also proven by H_2-TPD and EDX. Therefore, for the NiO/ZnO modified by TiO_2, it is more favorable to prepare the adsorbent by a kneading method for deep desulfurization.

In addition, it is also known from the H_2-TPR results that $NiO/ZnO-TiO_2$-**2** contained a lower content of free NiO, which was favorable for suppressing the olefin saturation reaction. The olefin contents of FCC gasoline before and after desulfurization on the two adsorbents are shown in Table 4. As demonstrated, the saturation amount of olefin in the FCC light gasoline after desulfurization on $NiO/ZnO-TiO_2$-**2** was smaller.

4. CONCLUSIONS

$NiO/ZnO-TiO_2$ adsorbents for FCC light gasoline desulfurization were prepared by the equal volume impregnation method ($NiO/ZnO-TiO_2$-**1**) and kneading method ($NiO/ZnO-TiO_2$-

Table 4. Olefin Content of FCC Gasoline before and after Desulfurization on the Two Adsorbents

samples	olefins (wt %)	alkane (wt %)	density (g/cm^3)
gasoline before desulfurization	42.6	55.27	0.6879
gasoline after desulfurization on Ni/ZnO-TiO$_2$-**1**	42.0	55.99	0.6763
gasoline after desulfurization on Ni/ZnO-TiO$_2$-**2**	42.3	55.10	0.6796

2). The NiO/ZnO-TiO₂-**2** adsorbent had a larger specific surface area and a smaller pore diameter than NiO/ZnO-TiO₂-**1** because the precursor of the active Ni species was uniformly mixed with the support powder in the NiO/ZnO-TiO₂-**2** adsorbent. Additionally, the NiO species was more uniformly dispersed and more Ni^0 active sites were generated on the surface of NiO/ZnO-TiO₂-**2**, which was responsible for its higher desulfurization performance than NiO/ZnO-TiO₂-**1**. The interaction between the active component and the support in the NiO/ZnO-TiO₂-**2** adsorbent was proven to be stronger so that the lower content free NiO was reduced, which was beneficial to suppress the olefin saturation in the desulfurization process. The final desulfurization results of the two adsorbents confirmed that the Ni/ZnO-TiO₂-**2** adsorbent was more excellent in both the desulfurization activity and suppression of olefin saturation.

■ AUTHOR INFORMATION

Corresponding Author

Weili Jiang − *College of New Energy and Materials, State Key Laboratory of Heavy Oil Processing, China University of Petroleum, Beijing 102249, China;* ⊙ orcid.org/0000-0002-7602-3343; Email: jiangweilipku@163.com

Authors

Guanglin Zhou − *College of New Energy and Materials, State Key Laboratory of Heavy Oil Processing, China University of Petroleum, Beijing 102249, China;* ⊙ orcid.org/0000-0002-5979-0057

Sheng Chen − *College of New Energy and Materials, State Key Laboratory of Heavy Oil Processing, China University of Petroleum, Beijing 102249, China*

Qin Li − *College of New Energy and Materials, State Key Laboratory of Heavy Oil Processing, China University of Petroleum, Beijing 102249, China*

Hongjun Zhou − *College of New Energy and Materials, State Key Laboratory of Heavy Oil Processing, China University of Petroleum, Beijing 102249, China;* ⊙ orcid.org/0000-0003-2927-0891

Xuecheng Gong − *College of New Energy and Materials, State Key Laboratory of Heavy Oil Processing, China University of Petroleum, Beijing 102249, China*

Xiance Zhang − *College of New Energy and Materials, State Key Laboratory of Heavy Oil Processing, China University of Petroleum, Beijing 102249, China*

Complete contact information is available at:
https://pubs.acs.org/10.1021/acsomega.1c06645

Notes

The authors declare no competing financial interest.

■ ACKNOWLEDGMENTS

■ REFERENCES

(1) Gu, X.; Yin, S.; Lu, X.; Zhang, H.; Wang, L.; Bai, L.; Wang, C.; Zhang, R.; Yuan, M. Recent development of a refined multiple air pollutant emission inventory of vehicles in the Central Plains of China. *J. Environ. Sci.* **2019**, *84*, 80−96.

(2) Nguyen, D. D.; Moghaddam, H.; Pirouzfar, V.; Fayyazbakhsh, A.; Su, C.-H. Improving the gasoline properties by blending butanol-Al₂O₃ to optimize the engine performance and reduce air pollution. *Energy* **2021**, *218*, No. 119442.

(3) Dehhaghi, M.; Kazemi Shariat Panahi, H.; Aghbashlo, M.; Lam, S. S.; Tabatabaei, M. The effects of nanoadditives on the performance and emission characteristics of spark-ignition gasoline engines: A critical review with a focus on health impacts. *Energy* **2021**, *225*, No. 120259.

(4) Zhan, X.; Sun, X. F.; Xu, H. L.; Li, J. D. Membrane materials for desulfurization of gasoline via pervaporation. *Prog. Chem.* **2019**, *31*, 752−759.

(5) Yu, F.; Wang, Q.; Li, G.; Yuan, B.; Xie, C.; Yu, S. Alkylation desulfurization of fcc gasoline over bronsted-lewis organic-inorganic heteropoly acid catalyst. *Chem. J. Chin. Univ.-Chin.* **2017**, *38*, 72−76.

(6) Ganiyu, S. A.; Ali, S. A.; Alhooshani, K. Simultaneous HDS of DBT and 4,6-DMDBT over single-pot Ti-SBA-15-NiMo catalysts: influence of Si/Ti ratio on the structural properties, dispersion and catalytic activity. *RSC Adv.* **2017**, *7*, 21943−21952.

(7) Yin, C.; Zhu, G.; Xia, D. A study of the distribution of sulfur compounds in gasoline fraction produced in China Part 2. The distribution of sulfur compounds in full-range FCC and RFCC naphthas. *Fuel Process. Technol.* **2002**, *79*, 135−140.

(8) Mirzoeva, L. M.; Ibragimova, M. D.; Nagiev, V. A.; Yunusov, S. G.; Andryushchenko, N. K.; Guseinov, G. D. Use of ionic liquids for desulfurization of gasoline fractions. *Chem. Technol. Fuels Oils* **2018**, *54*, 430−437.

(9) Yuan, P.; Lei, X.-Q.; Sun, H.-M.; Zhang, H.-W.; Cui, C.-S.; Yue, Y.-Y.; Liu, H.-Y.; Bao, X.-J.; Wang, T.-H. Effects of pore size, mesostructure and aluminum modification on FDU-12 supported NiMo catalysts for hydrodesulfurization. *Pet. Sci.* **2020**, *17*, 1737.

(10) Lin, W.; Fang, Y.; Li, X.; Zhou, Y. Preparation of Ni—Mo/γ-Al₂O₃ catalysts by vacuum impregnation and their use for hydrodesulfurization of dibenzothiophene. *Chem. Technol. Fuels Oils* **2017**, *53*, 779−786.

(11) Zheng, M.; Zhao, L.; Cao, L.; Zhang, Y.; Gao, J.; Xu, C. Insights into the HDS/HYDO selectivity with considering stacking effect of Co-MoS₂ catalysts by combined DFT and microkinetic method. *Fuel* **2021**, *300*, 120941.

(12) Jiang, W.; Gao, X.; Dong, L.; Xiao, J.; Zhu, L.-H.; Chen, G.-Y.; Xun, S.-H.; Peng, C.; Zhu, W.-S.; Li, H.-M. Aerobic oxidative desulfurization via magnetic mesoporous silica-supported tungsten oxide catalysts. *Pet. Sci.* **2020**, *17*, 1422−1431.

(13) Ahmad, W.; Ur Rahman, A.; Ahmad, I.; Yaseen, M.; Mohamed Jan, B.; Stylianakis, M. M.; Kenanakis, G.; Ikram, R. Oxidative desulfurization of petroleum distillate fractions using manganese dioxide supported on magnetic reduced graphene oxide as catalyst. *Nanomaterials* **2021**, *11*, 203.

(14) Ju, F.; Liu, C.; Meng, C.; Gao, S.; Ling, H. Reactive adsorption desulfurization of hydrotreated diesel over a Ni/ZnO-Al₂O₃-SiO₂ adsorbent. *Energy Fuels* **2015**, *29*, 6057−6067.

(15) Yun, X. Study on reaction of thiophene compounds and olefins for deep desulfurization of gasoline. *China Pet. Process. Petrochem. T.* **2019**, *21*, 53−60.

(16) He, E.; Huang, G.; Fan, H.; Yang, C.; Wang, H.; Tian, Z.; Wang, L.; Zhao, Y. Macroporous alumina- and titania-based catalyst for carbonyl sulfide hydrolysis at ambient temperature. *Fuel* **2019**, *246*, 277−284.

(17) Guan, X.; Wang, Y.; Cai, W. A composite metal-organic framework material with high selective adsorption for dibenzothiophene. *Chin. Chem. Lett.* **2019**, *30*, 1310−1314.

(18) Wang, T.; Wang, X.; Gao, Y.; Su, Y.; Miao, Z.; Wang, C.; Lu, L.; Chou, L.; Gao, X. Reactive adsorption desulfurization coupling aromatization on Ni/ZnO-Zn₆Al₂O₉ prepared by ZnxAly-(OH)₂(CO₃)ₓcenter dot xH₂O precursor for FCC gasoline. *J. Energy Chem.* **2015**, *24*, 503−511.

(19) Zu, Y.; Zhang, C.; Qin, Y.; Zhang, X.; Zhang, L.; Liu, H.; Gao, X.; Song, L. Ultra-deep adsorptive removal of thiophenic sulfur compounds from FCC gasoline over the specific active sites of CeHY zeolite. *J. Energy Chem.* **2019**, *39*, 256−267.

(20) Liu, Y.; Pan, Y.; Wang, H.; Liu, Y.; Liu, C. Ordered mesoporous Cu-ZnO-Al$_2$O$_3$ adsorbents for reactive adsorption desulfurization with enhanced sulfur saturation capacity. *Chin. J. Catal.* **2018**, *39*, 1543−1551.

(21) Deng, J.; Wang, Q.; Zhou, Y.; Zhao, B.; Zhang, R. Facile design of a ZnO nanorod-Ni core-shell composite with dual peaks to tune its microwave absorption properties. *RSC Adv.* **2017**, *7*, 9294−9302.

(22) Chen, W.-C.; Yu, X.-L.; Huang, H.; Shi, L.; Meng, X. Effect of Mixed Oxide Support for Ni/ZnO in Reactive Adsorption Desulfurization. *China Pet. Process. Petrochem. T.* **2016**, *18*, 11−18.

(23) Jin, S.; Yue, Q.; Meng, T.; Zhang, H.; Jiang, N.; Jin, M.; Zhang, R. Ultra-deep desulfurization via reactive adsorption on nickel and zinc species supported on activated carbon. *J. Porous Mat.* **2017**, *24*, 1697−1704.

(24) Lyu, Y.; Sun, Z.; Meng, X.; Wu, Y.; Liu, X.; Hu, Y. Scale-up reactivation of spent S-Zorb adsorbents for gasoline desulfurization. *J. Hazard. Mater.* **2022**, *423*, 126903.

(25) Ganiyu, S. A.; Lateef, S. A. Review of adsorptive desulfurization process: Overview of the non-carbonaceous materials, mechanism and synthesis strategies. *Fuel* **2021**, *294*, No. 120273.

(26) Babich, I. V.; Moulijn, J. A. Science and technology of novel processes for deep desulfurization of oil refinery streams: A review. *Fuel* **2003**, *82*, 607−631.

(27) Ullah, R.; Bai, P.; Wu, P.; Zhang, Z.; Zhong, Z.; Etim, U. J.; Subhan, F.; Yan, Z. Comparison of the reactive adsorption desulfurization performance of Ni/ZnO-Al$_2$O$_3$ adsorbents prepared by different methods. *Energy Fuels* **2016**, *30*, 2874−2881.

(28) Meng, X.; Huang, H.; Weng, H.; Shi, L. Ni/ZnO-based Adsorbents Supported on Al$_2$O$_3$, SiO$_2$, TiO$_2$, ZrO$_2$: A Comparison for desulfurization of model gasoline by reactive adsorption. *Bull. Korean Chem. Soc.* **2012**, *33*, 3213−3217.

(29) Huang, L.; Ge, H.; Yan, L. Desulfurization of diesel over Ni/ZnO adsorbent prepared by coprecipitation. *Russ. J. Appl. Chem.* **2018**, *91*, 833−838.

(30) Jiang, W.; Chen, Y.; Gao, L.; Sun, M.; Wang, X.; Li, Z.; Ji, X.; Zhou, G.; Zhou, H. Hydroformylation for reducing the olefin content in the FCC light gasoline with magnetic rhodium-catalysts. *Fuel* **2020**, *279*, No. 118508.

(31) Zhou, W.; Yang, L.; Liu, L.; Chen, Z.; Zhou, A.; Zhang, Y.; He, X.; Shi, F.; Zhao, Z. Synthesis of novel NiMo catalysts supported on highly ordered TiO$_2$-Al$_2$O$_3$ composites and their superior catalytic performance for 4,6-dimethyldibenzothiophene hydrodesulfurization. *Appl. Catal., B* **2020**, *268*, No. 118428.

(32) Chen, S.; Li, Q.; Wang, X.; Gong, X.; Jiang, W.; Zhou, G. Effect of Ti doping on Ni/ZnO-TiO$_2$ adsorbent for desulfurization performance of FCC light gasoline. *Acta Pet. Sin. (Pet. Process. Sect.)* **2020**, *36*, 388−395.

(33) Ju, F.; Wang, M.; Luan, H.; Du, P.; Tang, Z.; Ling, H. Reactive adsorption desulfurization of NiO and Ni-o over NiO/ZnO-Al$_2$O$_3$-SiO$_2$ adsorbents: role of hydrogen pretreatment. *RSC Adv.* **2018**, *8*, 33354−33360.

(34) Tang, M. X.; Zhou, L. G.; Du, M. X.; Lyu, Z. J.; Wen, X. D.; Li, X. K.; Ge, H. A novel reactive adsorption desulfurization Ni/MnO adsorbent and its hydrodesulfurization ability compared with Ni/ZnO. *Catal. Commun.* **2015**, *61*, 37−40.

(35) Ullah, R.; Bai, P.; Wu, P.; Etim, U. J.; Zhang, Z.; Han, D.; Subhan, F.; Ullah, S.; Rood, M. J.; Yan, Z. Superior performance of freeze-dried Ni/ZnO-Al$_2$O$_3$ adsorbent in the ultra-deep desulfurization of high sulfur model gasoline. *Fuel Process. Technol.* **2017**, *156*, 505−514.

(36) Weng, X.; Cao, L.; Zhang, G.; Chen, F.; Zhao, L.; Zhang, Y.; Gao, J.; Xu, C. Ultradeep hydrodesulfurization of diesel: mechanisms, catalyst design strategies, and challenges. *Ind. Eng. Chem. Res.* **2020**, *59*, 21261−21274.

(37) Fernandes, D. M.; Scofield, C. F.; Neto, A. A.; Cardoso, M. J. B.; Zotin, J. L.; Zotin, F. M. Z. The hydrogen adsorption capacity of commercial Pd/Rh and Pt/Rh automotive catalysts and its relationship to their activity. *Chem. Eng. J.* **2012**, *189-190*, 62−67.

(38) Velu, S.; Gangwal, S. K. Synthesis of alumina supported nickel nanoparticle catalysts and evaluation of nickel metal dispersions by temperature programmed desorption. *Solid State Ionics* **2006**, *177*, 803−811.